Clément Michoud · Valérie Baumann · Tom Rune Lauknes · Ivanna Penna · Marc-Henri Derron · Michel Jaboyedoff

Large slope deformations detection and monitoring along shores of the Potrerillos dam reservoir, Argentina, based on a small-baseline InSAR approach

Abstract The Argentina National Road 7 that crosses the Andes Cordillera within the Mendoza province to connect Santiago de Chile and Buenos Aires is particularly affected by natural hazards requiring risk management. Integrated in a research plan that intends to produce landslide susceptibility maps, we aimed in this study to detect large slope movements by applying a satellite radar interferometric analysis using Envisat data, acquired between 2005 and 2010. We were finally able to identify two large slope deformations in sandstone and clay deposits along gentle shores of the Potrerillos dam reservoir, with cumulated displacements higher than 25mm in 5years and towards the reservoir. There is also a body of evidences that these large slope deformations are actually influenced by the seasonal reservoir level variations. This study shows that very detailed information, such as surface displacements and above all water level variation, can be extracted from spaceborne remote sensing techniques; nevertheless, the limitations of InSAR for the present dataset are discussed here. Such analysis can then lead to further field investigations to understand more precisely the destabilising processes acting on these slope deformations.

Keywords Slope deformations · Detection · Monitoring · InSAR · Small baseline · Dam reservoir · Argentina

Introduction

Landslide susceptibility mapping at regional scale is the starting point to detect areas exposed or potentially exposed to natural hazards, and it is an essential support for hazard and risk assessment. In particular, the detection of active and large instabilities is decisive since these deformations can turn into rapid movements such as spreads, rockfalls or even rock avalanches (Crosta et al. 2013) that may affect infrastructures and/or population.

Landslide inventories constitute thus key baseline information during hazard assessments (Fell et al. 2008; Guzzetti et al. 2012). A classic approach to perform inventories is to use aerial photos, as these pictures provide an overall point of view of a large area (Rib and Liang 1978; Záruba and Mencl 1982). Nowadays, aerial laser scanning (ALS) is widely used to produce high-resolution digital elevation models (HRDEM) at regional scales; HRDEM have then become an essential input data of regional landslides inventory maps (Chigira et al. 2004; McKean and Roering 2004; Ardizzone et al. 2007; Jaboyedoff et al. 2012; Pedrazzini 2012). Their high level of detail allows indeed to identify main morphostructural features developed as a result of slope deformations, such as crowns, counterscarps, double ridges or trenches being created by deep-seated slope deformations (DSGSD, e.g. Chigira 1992; Agliardi et al. 2001; Braathen et al. 2004; Crosta et al. 2013; Hungr et al. 2014).

In addition to aerial imaging and HRDEM, satellite interferometric synthetic aperture radar (InSAR) can also be used to update inventories and states of activities of slow slope deformations, as the method has proven suitable to detect and monitor extremely slow rotational slides, topples and spreads at regional scales (Massonnet and Feigl 1998; Lauknes et al. 2010; Henderson et al. 2011). The main principle of radar interferometry is based on studying the phase difference between two different synthetic aperture radar (SAR) images (Massonnet and Feigl 1998; Bamler and Hart 1998). The main applications of InSAR are generation of topographic models (Shapiro et al. 1972) and studies of surface deformations (Massonnet 1985; Gabriel et al. 1989), applied to crustal deformations (Massonnet et al. 1993; Massonnet et al. 1995; Sigmundsson et al. 1997) or even to landslides (Fruneau and Apache 1996; Carnec et al. 1996; Kimura and Yamaguchi 2000; Squarzoni et al. 2003; Berardino et al. 2003; Saroli et al. 2005; Yin et al. 2010; García-Davalillo et al. 2014).

However, single interferograms are often difficult to interpret due to phase propagation delays related to different atmospheric conditions (Tarayre and Massonnet 1996; Zebker et al. 1997; Hanssen 2001; Doin et al. 2009). In the last decade, new algorithms have been developed, such as persistent scatterer interferometry (PSI) (Ferretti et al. 2001), small baselines (SBAS) (Berardino et al. 2002) or SqueeSAR (Ferretti et al. 2011). They aim to improve the reliability of measures by separating movement signals from typical noise sources and to provide temporal evolution of deformation behaviours. For example, the SBAS technique stacks and filters multi-temporal interferograms with small spatial baselines, increasing the signal/noise ratio (SNR) allowing tracking of temporally coherent distributed scattering.

These advanced algorithms are then frequently used for accurate landslide mapping and monitoring (e.g. Colesanti and Wasowski 2006; Fornaro et al. 2009; Herrera et al. 2011 and 2013; Lauknes et al. 2010; Bianchini et al. 2012; Cigna et al. 2013; Crosta et al. 2013; Bardi et al. 2014). Nevertheless, they are still often used as a complementary material to support pre-existing inventories updating state of activities of detected landslides (Guzzetti et al. 2012), since advanced InSAR techniques do not usually detect more than 50 % (e.g. in Bianchini et al. 2012; Herrera et al. 2013) of instabilities in rough relief terrains. It is mainly explained by (1) undetectable areas on westward and eastward slopes that are invisible by the SAR sensor stemming from geometric and radiometric distortions and (2) undetectable deformations on northward and southward slopes since they are easily perpendicular to the sensor line of sight (LOS) in both ascending and descending acquisition orbits (Hanssen 2001; Woodhouse 2006; Cascini et al. 2009). In addition, the ratio of detected landslides by such techniques can even be lower in densely vegetated areas, affected by strong decorrelations.

Following these statements, we carried out large slope deformation detections along the Argentinean National Road 7 (N7) within the Mendoza province, Argentina. The N7 is indeed an

essential corridor of Southern America, linking Buenos Aires to Santiago de Chile by crossing the Andes Cordillera at the Cristo Redenor international pass up to 3200 m a.s.l. At least 2200 cars and trucks use the road every day (Dirección Nacional de Vialidad 2013). At the same time, this road section along the Mendoza River is exposed to numerous natural hazards and remains therefore frequently closed by snow and landslides (Baumann et al. 2005). It represents a risk for road users that must be considered, and it also implies regional economic losses in case of prolonged road closure. Furthermore, the N7 follows the south-western reservoir shores of the Potrerillos hydropower dam (fully operational since the mid-2000s), which is a main source of drinking water and energy for the Mendoza city, as well as a touristic site. As reservoir–landslides interactions were reported in many investigations worldwide (Terzaghi 1950; Müller 1964; Riemer 1995; Wang et al. 2008; Schuster 2006; Bell 2007; Pinyol et al. 2012; Xia et al. 2013) and were monitored with SAR techniques (Fu et al. 2010; Singleton et al. 2014; Tomás et al. 2014), slope deformation may also affect the N7 close to the reservoir.

In this context, a long-term project, initiated by the Argentinean Geological Survey and the University of Lausanne, plans to produce inventory and susceptibility maps for snow avalanches, debris flows, rockfalls and slides (Wick et al. 2010a,b; Baumann et al. 2011) along the N7, between Potrerillos and Las Cuevas near the Chilean border (Fig. 1), by means of remote sensing and regional numerical modelling approaches coupled with classical field survey (Jaboyedoff et al. 2012). Within this framework, this study aims to invent large slope deformations; but without available HRDEM and orthophoto, a small baseline (SBAS) approach (Berardino et al. 2002) has hence been selected to detect as much large mass movements as possible, since the main

landscapes with low and sparse vegetation and many outcrops (Fig. 1) constitute relevant distributed scatterers (Lauknes et al. 2010).

In this paper, we therefore present results based on active mass movement detection by SBAS processing of ESA's Envisat satellite SAR images between Potrerillos and Uspallata, with a specific focus along shores of the Potrerillos dam reservoir where large slope deformations have been detected and monitored.

General setting

Morphotectonic context

The study area extends along two main morphotectonic units named from west to east: Cordillera Frontal and Precordillera; both are separated by an intermountain valley (Fig. 1). Here, the tectonic style of the eastern Andes is strongly influenced by morphological and tectonic features related to Triassic and Paleozoic structures, reactivated during the Cenozoic (Kozlowski et al. 1993). In this region, oblique thrust fault structures with NW and NNW directions are widespread. In the following paragraphs, we describe main characteristics of these units:

1. The Frontal Cordillera was uplifted during the Neogene by high-angle east-vergent reverse faults (Ramos 1997). Main outcrops correspond to the Permian–Triassic Choiyoi Group, composed of extrusive and intrusive igneous rocks. The relief of the Cordillera Frontal results from high-rate uplift since the Neogene, and glacial and fluvial incision. Landscape was shaped by glaciers during Quaternary times, whereas current glaciers are constrained to a reduced area at high altitudes
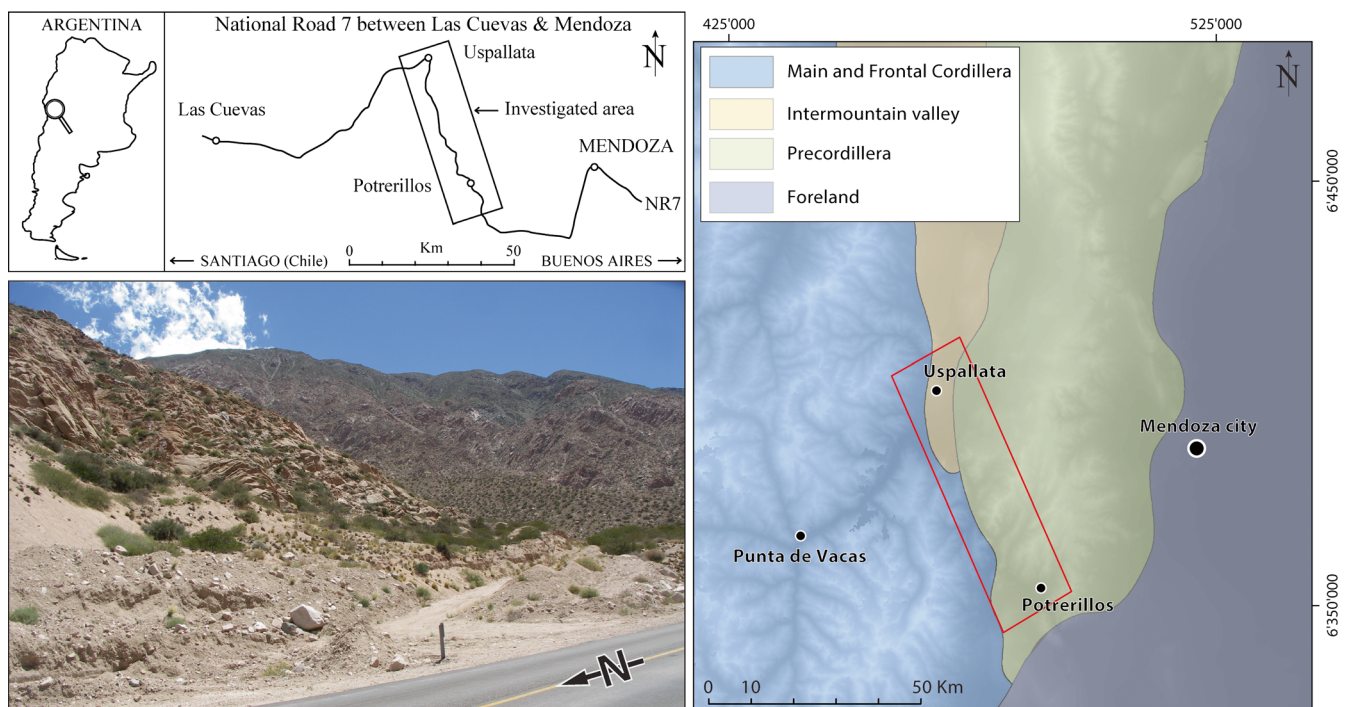

Fig. 1 *Upper left* Location of the study area within the Mendoza Province. *Lower left* Illustration of the dominant landscape along the N7 corridor, where a rocky landscape with low and sparse vegetation is observed. *Right* Main morphotectonic units comprised in the study area

(3800 m a.s.l.; Trombotto and Borzotta 2009). Glacial retreat and seismic activity were proposed as conditioning factors of large slope collapses that have taken place in Holocene times (Hermanns et al. 2014).

2. The Precordillera corresponds to a fold and thrust belt structured by east and west-vergent basement faults deforming Proterozoic to Neogene metamorphic and sedimentary rocks (Giambiagi and Martinez 2008). In the Potrerillos area, Triassic conglomerates, sandstones, mudstones and volcaniclastics rocks uncomfortably overlay the Permian–Triassic volcaniclastic rocks from Choiyoi Group (Stipanicic 1979). On South and East of Potrerillos lake, outcrops are Neogene sedimentary rocks (Folguera et al. 2003). Here, it is observed a dense drainage networks composed of slightly permanent or ephemeral colluvial creeks and gullies that give place to a rough landscape. The slopes are characterised by low gradients, where an erosive surface developed on Triassic to Tertiary sedimentary rocks. The eastern foothills show wide alluvial deposits belonging to different aggrading levels (Polansky 1963).

Between Uspallata and Potrerillos, the Mendoza River crosses the Frontal Cordillera and Precordillera with NW–SE direction. The Mendoza River here has an anastomotic pattern with, in addition, three main levels of terraces. At both sides of the valley, alluvial and colluvial fans are observed at the mouth of tributary rivers, as well as talus at the toe of rockslopes. Pediments surface with at least three different levels are well developed in the Potrerillos area (Fig. 2).

Landscape and active surface processes

The landscape presents maximum elevations of 5400 m a.s.l. and lower at around 1500 m a.s.l. Weather is characterised by arid and semi-arid conditions, with mean annual rainfall of 140–360 mm (Subsecretaría de Recursos Hídricos 2013). Most of the storms take place during October–March, and from June to August is the period of high snow fall. Mean temperature varies with altitude, between 1200 and 3800 m a.s.l., namely, 20 and 4 °C in summer and 5 and −7 °C in winter (Fernández García and Polimeni 2003). The vegetation is sparse and mainly composed of thorny thickets, grass family and cactuses.
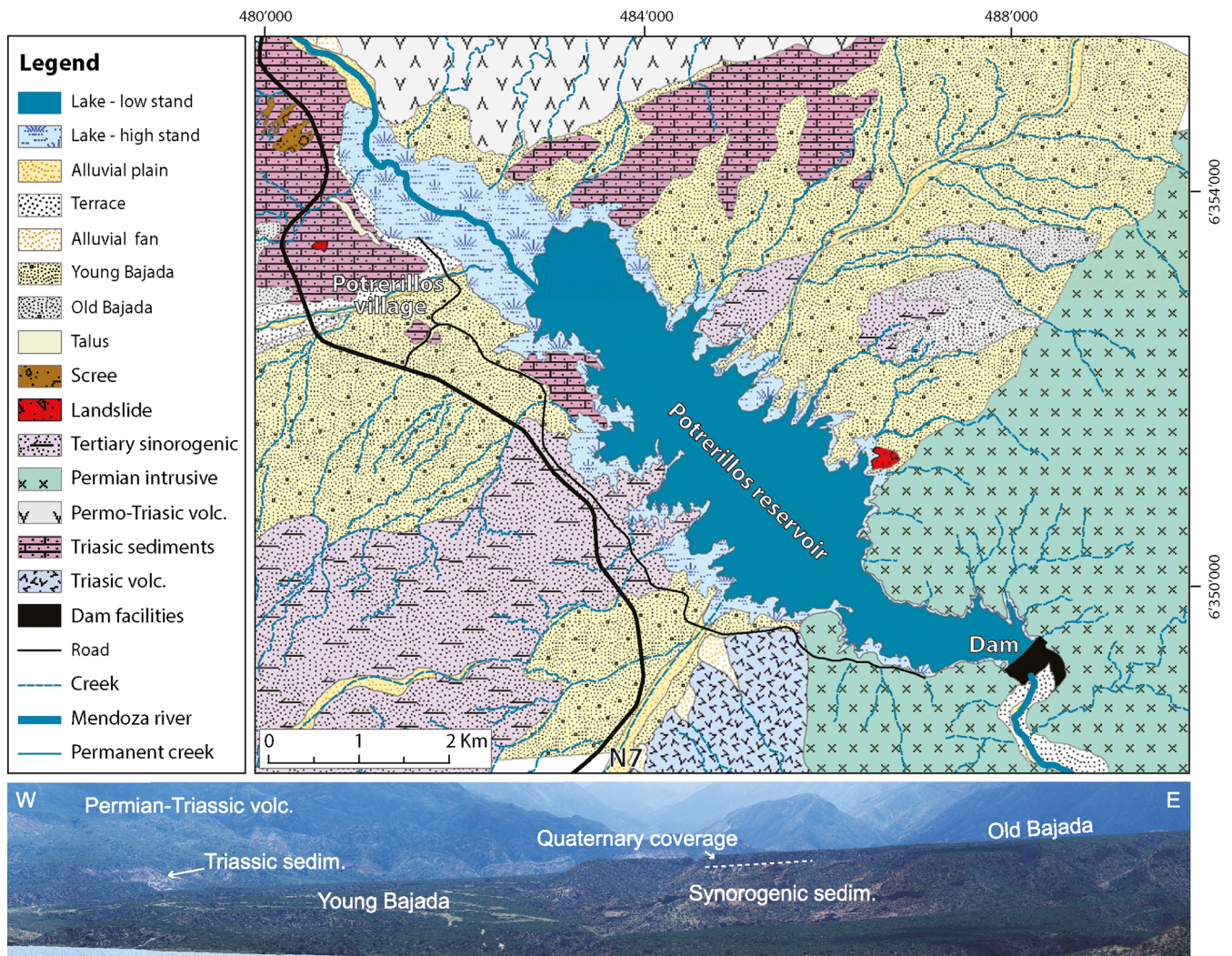

Fig. 2 Geomorphologic map of the Potrerillos area (ages of units taken from Giambiagi et al. 2011), and Panorama picture of the north-eastern margin of the lake showing main geomorphologic and geologic units. The mapped landslide refers to the one described in the 'General setting' of the supplementary material

U-shaped valleys are observed at high altitude, and in some places, rock glaciers remain. At lower altitudes, landscape is dominated by fluvial action (Folguera et al. 2003). At Uspallata, the Mendoza River runs in a NE–SW direction, and then turns to the SE up to Potrerillos area, where a hydropower dam was built, creating a permanent water body extending around 9 km along the Mendoza valley (Fig. 2).

Due to its tectonic and geomorphic history, the area has been active in terms of hillslope processes. Several large magnitude slope collapses have taken place during Holocene times. Eight rock avalanches with volumes of several million cubic metres were indeed mapped near Uspallata. Their detachment was located along the Carrera fault system and involved Permo-Triassic volcanic rocks of the Choiyoi Group (Fauqué et al. 2000). In addition, a large landslide was also recognised near the northern shore of the Mendoza river, 22 km upstream the Potrerillos reservoir (Fauqué et al. 2005). While these mass movements are proposed to be conditioned by active tectonic conditions, those located to the west of Uspallata, near Punta de Vacas in the Frontal Cordillera, have been proposed to be linked to debuttressing of valley flanks after the glacial retreat (Fauqué et al. 2000, 2005; Cortés et al. 2006; Hermanns et al. 2014).

Current active surface processes involve mainly snow avalanches, debris flows and rockfalls. Every year, the N7 is affected by several events from Potrerillos to Chile (Baumann et al. 2005, 2011; Moreiras 2005, 2006; Wick et al. 2010a,b). For example, in 2005, a 7×10^4 m³ debris flow covered the N7 at the Guido's curve along 300 m, hitting a car and stopping 3000 vehicles during 12 h (Wick et al. 2010b). Moreover, a large rock fall (<100 m³) occurred in 2011 near the Guido's curve from an anthropic road cut slope in volcanic rocks reached the way and caused one fatality. In addition, in the Potrerillos area, rockfalls are widespread recorded along cut overdip slopes on soft Triassic and Neogene sandstones and conglomerates. Morphology conditions, degree of rocks fracturing, amounts of sediments stored on watersheds and also unstably designed cut-slope design are the main conditioning factors of these active processes; they are mostly triggered by rainfall and snow melting, but earthquakes have also generated rock falls in the area (Wick et al. 2010a).

SAR data processing

Available SAR data

Our analysis is based on 47 SAR images acquired by the European Space Agency (ESA) Envisat ASAR instrument. The scenes cover the road section Mendoza–Uspallata during the 2005–2010 period from both ascending and descending orbits (Fig. 3).

The 27 ascending scenes (track 447, frame 6525) were acquired from January 2005 to November 2006 and June 2009 to February 2010, whereas the 20 descending scenes (track 425, frame 4278) are from September 2007 to January 2010 (Table 1). Finally, the 90 m DEM acquired by the SRTM mission in 2000 (Jarvis et al. 2008) will be used to filter unwanted topographic- and atmospheric-related contributions.

Landslides detection at regional scale

Regional SBAS processing
The Norut *GSAR* software (Larsen et al. 2005; Lauknes et al. 2010) has been used for all InSAR processing, following the principal steps described hereafter. Main settings are summarised in Table 2.

For each dataset, raw SAR images are first focussed to single-look complex and then co-registered to ensure a perfect overlap between pixels from the different scenes in SAR geometry.

Regarding the ascending scenes, 107 interferograms with temporal and normal baselines lower than 1200 days and 400 m are computed (Fig. 4a). In addition, 58 interferograms are calculated comparing the descending scenes having temporal and normal baselines lower than 400 days and 230 m (Fig. 4b); smaller baselines were optimised for this second dataset since the descending acquisitions had shorter spatial and temporal baselines. For each interferogram, the topography-related phase was removed from the external SRTM DEM using mathematical developments defining InSAR signal construction and simulating the DEM signal response (more details available in, e.g. Massonnet and Feigl 1998; Hanssen 2001; Woodhouse 2006).

However, phase propagation delays created by temporal changes in atmospheric conditions within the troposphere between SAR acquisitions and orbital correction errors can still introduce artefacts and hamper interpretation (Zebker et al. 1997; Hanssen 2001). Interferograms too much affected by these artefacts were removed from the study using manual inspection; all interferograms having large areas with incoherent noise and no well-defined fringe patterns were deleted. Finally, 57 ascending and 36 descending interferograms were selected for processing.

The phase unwrapping step, which converts each ambiguous 2π cycle to absolute value of interferometric phase, is performed with the *SNAPHU* software (Chen and Zebker 2001). Prior to this step, noisy areas have been masked out in order to ensure a suitable continuity of values with a good enough coherence to be interpreted. Pixels with coherence lower than 0.35 on 50 % of interferograms were thus masked out, which are about 66 % of pixels of ascending interferograms and 50 % of pixels of descending ones.
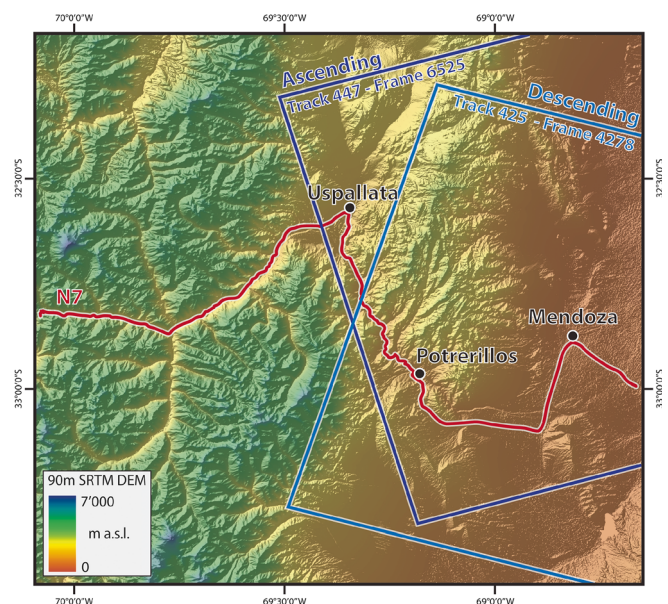

Fig. 3 Frames of the Envisat ASAR ascending and descending scenes of the study area, wrapped on the 90 m SRTM DEM used for the SBAS processing. (Raw Envisat data: ©ESA 2010; raw DEM data: ©SRTM NASA)

Table 1 Envisat's tracks/frames 447/4278 and 425/6525 of SAR scenes provided by the ESA for this study (ESA Category-1 Project 7154)

Dates for ascending scenes (yyyy.mm.dd)	Dates for descending scenes (yyyy.mm.dd)
2005.01.11	2007.09.19
2005.02.18	2007.11.28
2005.03.25	2008.01.02
2005.04.29	2008.02.06
2005.06.03	2008.03.12
2005.07.08	2008.04.16
2005.08.12	2008.06.25
2005.09.16	2008.07.30
2005.10.21	2008.09.03
2005.11.25	2008.10.08
2006.02.03	2008.11.12
2006.03.10	2009.02.25
2006.04.14	2009.04.01
2006.05.19	2009.05.06
2006.06.23	2009.06.10
2006.07.28	2009.07.15
2006.09.01	2009.08.19
2006.10.06	2009.09.23
2006.11.11	2009.10.28
2008.04.18	2010.01.06
2009.06.12	
2009.07.17	
2009.08.21	
2009.09.25	
2009.12.04	
2010.01.08	
2010.02.12	

InSAR-based results are relative displacements between scatterers that need to be calibrated to get absolute ground movements. To do that, a common reference area (for which we assume no movements) is used for both ascending and descending processing. Ideally, this pixel must be in a stable place, close to the study area and inside a cluster of several very coherent pixels; the pixel should also be in an area that remain stable when fixing the reference in different places during prior test processing. For these reasons, we selected a coherent point within an assumed stable area in the northern–western part of the Potrerillos reservoir and close to the N7 (Fig. 5, and Figure 1 of the supplementary material). Finally, the stacks of unwrapped interferograms were inverted to extract time-series displacements and mean velocity for each pixel by applying the SBAS method.

Results of the regional approach

Figure 5 displays the mean displacement velocities measured in the satellite line of sight direction (LOS), extracted from the ascending SBAS processing. We assume here that the largest part of the whole processed study area, mainly composed of Triassic to Neogene sedimentary rocks in the Foreland plains (Folguera et al. 2003), is not affected by large slope instabilities and that no regional tectonic deformations affect SBAS results (cf. 'Influences of the Andean orogen'); pixels from stable areas should thus constitute the highest majority of the coherent reflectors. Furthermore, we notice that both processed mean LOS velocities can be fitted by normal distributions; velocities of stable pixels, theoretically close 0 mm/year, thus fix the mean of the normal distribution. As a result, by highlighting reflector clusters having velocities within high standard deviation ranges (>2σ), we detect either areas affected by strong artefacts or large slope displacements (Fig. 5).

We also remark that ascending results are less noisy than the descending ones, since the mean LOS velocity of all scatterers has a median and standard deviations of −1.2 and 2 mm/year, instead of −7 and 11 mm/year. Then, regarding the spatial distribution of the about 2.4 million coherent points of ascending and descending processing, we can state that point density is relatively high on the eastward and northward plains. It corresponds to areas with good coherence. On the contrary, elevated and steeply sloping regions have only sparse reflectors; the majority of them were indeed masked out since there coherence was lower than 0.35. This is probably due to steepness of terrain introducing radar geometrical effects such as foreshortening and shadowing and also due to low coherence because of snow cover.

Regarding our region of interest, between Potrerillos and Uspallata, no cluster with significant velocity deviations imputed to slope instabilities can be thus detected, since pixels on steep slopes along the N7 corridor are indeed masked out (cf. 'Limitations to large landslides detection'). But, in the meantime, although no clear evidences of large landslides can be noticed on noisy descending results (Figure 1 of the supplementary material), we observe on ascending ones several distinct downward mass movements along gentle shores of the Potrerillos earth dam reservoir (Fig. 5). Since these deformations may affect the N7, focussed investigations are then achieved.

Landslide monitoring along shores of the Potrerillos' dam reservoir

Local SBAS processing

A focussed SBAS processing is now carried out on this Potrerillos reservoir area. Main settings described in 'Regional SBAS processing' and Table 2 (such as maximal temporal and spatial baselines and coherence thresholds) are again applied. Nevertheless, the selection of interferometric pairs showing coherent signal within this smaller region of interest was optimised for this local study in order to extract displacement time series as reliable as possible. We indeed select 75 ascending and 57 descending interferograms; in addition, the reference point of the ascending processing was set

Table 2 Main set parameters for SBAS processing with the *GSAR* software

	Ascending scenes		Descending scenes	
	Regional	Local	Regional	Local
Size of scenes	47×140 km	10×8 km	46×92 km	37×32 km
Number of scenes	27		20	
Look azimuth-angle	074°27°		286°30°	
Max. temporal baseline	1200 days		400 days	
Max. normal baseline	400 m		230 m	
Number of total interferograms	107		58	
Number of selected interferograms	57	75	36	23
Coherence thresholds	0.35 on 50 % of interferograms			
Reference point (UTM19° S)	481'386 6'353'063	481'360 6'353'051	479'424 6'356'660	479'452 6'356'672
Number of reflectors	2'300'000	38'000	2'400'000	340'000

in the new Potrerillos village in a cluster of very coherent pixels where no significant displacement was identified on regional results. For the same reasons, the reference point of the descending processing was set 2.5 km westwards from the Potrerillos village.

Detection and monitoring results

On the ascending results, two large mass movements with areas above the water level of about 2.5 and 0.7 km² are detected on the western and eastern shores of the lake. Both have cumulated displacements higher than 30 mm in 5 years (Fig. 6), and their velocity gradients suggest a general dip direction toward the reservoir. Smaller and slower movements are also noticed on the north-eastern and southern shores.

Displacement time series furthermore confirm reliable patterns with constant and progressive movements during periods 2005–2006 and 2009 (when we got one acquisition each month), with mean velocities of about 8 mm/year and up to 20 mm/year, respectively (Fig. 6). On the contrary, almost no displacements are extracted in 2007–2008, since having only one acquisition in 2 years increases significantly the fringe ambiguity potential issues (Woodhouse 2006). The total cumulated displacement measured on the ascending data, up to 30 mm in both large mass movements, is thus probably underestimated.

However, results from descending scenes (Figure 2 of the supplementary material) seem to be noisier with cumulated errors inside areas assumed as stable varying between about [−7;7]mm in 2.5 years, instead of [−5;5]mm in 5 years for the ascending interferograms. Moreover, the eastern deformation mapped in Fig. 6 is not detected on this processing, and the western one is only detected on its upper part within a larger and slower mass movement.

Their mechanisms and geometries (identified as deep extremely slow soft rock rotational and also translational slides) are afterward discussed in 'SBAS-derived geometry'.

Water level fluctuations of the reservoir

In order to study potential reservoir–landslides interactions, as it has been reported in many investigations worldwide since Terzaghi 1950, the water level variation along time of the Potrerillos reservoir has been surveyed and extracted from SAR return amplitude images (Fig. 7). These variations are first qualitatively assessed by comparing the reservoir surface changes along time. Indeed, the larger the reservoir area is, the higher the water level is (López et al. 2011). Afterwards, we select on each of the 47 amplitudes images 16 pixels well distributed along the reservoir shoreline, and we estimate their elevation by overlapping these images on the SRTM DEM. We compute for all scenes the median (attenuating extreme value effects; Höhle and Höhle 2009) and the standard deviation of the 16 values; we then delete outliers and compute again filtered standard deviation, in order to decrease errors introduced by the SRTM model and sometimes unclear limits between water and land at a pixel scale. The water level variation of the reservoir along time is finally assessed by connecting all median elevations while first qualitative observations must be respected.

As a result, we notice that the water level is varying along time between −25 and +15 m around a mean level that makes a range of elevation of about 40 m, actually close to the 44 m (minimum and maximum levels are respectively at 1342 and 1386 m a.s.l.) stated in López et al. (2011). The reservoir level, artificially regulated, is usually high from February to August. It quickly draws down afterwards till December, and is then filled till the beginning of February, fed by usual high discharge peaks of the Río Mendoza in December and January due to the snow melting in the high river watershed (Subsecretaría de Recursos Hídricos 2013).

Discussion

Influences of the Andean orogen

Mendoza regions are subjected to tectonic uplift resulting from the compressive strains formed because of the subduction of the

A (Ascending: $Bt_{max}= 1'200$ days , $Bn_{max}= 400$ m)

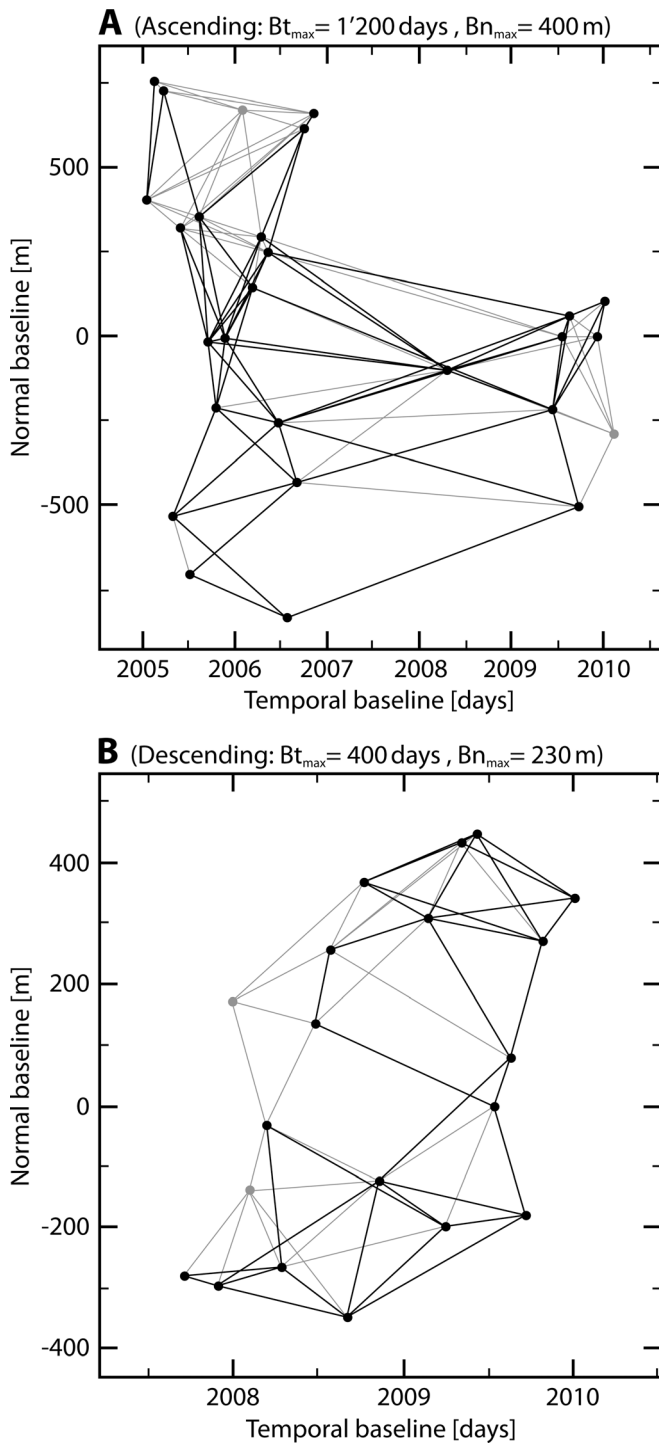**B** (Descending: $Bt_{max}= 400$ days , $Bn_{max}= 230$ m)

Fig. 4 Normal baselines vs. temporal baselines plot **a** of the 107 interferometric ascending pairs using thresholds of 1200 days and 400 m, and **b** of the 58 interferometric descending pairs using thresholds of 400 days and 230 m. Every line corresponds to a computed interferogram between two acquisitions; *black lines* correspond to interferograms kept after selection, while the *grey lines* are the non-selected ones

Nazca plate beneath the Sudamerican plate, which gives place to the Andean Mountains. The southern section of the central Andes

is hence affected by significant Eastward shortening rates caused by episodic release of transient elastic deformations during large earthquakes and by permanent displacements due to the Pampean flat-slab and the mountain uplift (Gansser 1973; Ramos 1999). GNSS measurements are showing north-eastward displacement rates between about 7.3 mm/year at San Juan and 19.4 mm/year at Santiago de Chile (Kendrick et al. 1999).

These deformations are supposed to be uniform within our study area, since its extent is relatively small compared to the continental scale of the Andean orogen. This subduction component is therefore implicitly deleted at the beginning of the SBAS processing by focussing and co-registering the successive SAR scenes that might be translated by continuous mm displacements (cf. 'Regional SBAS processing') and is de facto not considered.

Limitations to large landslide detection

Regional mean LOS velocities are correlated with the scatters' azimuth (in SAR geometry) and elevation on both regional processing. As illustrated in Fig. 8, quadratic polynomial trends can indeed be fitted.

As we assume no influence of the Andean tectonic (cf. 'Influences of the Andean orogen'), these correlations result from two main uncertainty sources in the input data. Firstly, the correlation of mean LOS velocities and azimuthal pixel coordinates may be misinterpreted as a regional N–S displacement trend, but it should actually be attributed to orbital errors. Inaccurate Envisat trajectories estimations with errors higher than 3 m are indeed a common source of residual fringes on interferograms (Hanssen 2001) unrelated to any real ground movements. Secondly, the refractivity index of the atmosphere varies vertically, mainly because the successive horizontal layers of the stratified troposphere have specific water vapour pressures (Hanssen 2001). Differential vertical phase delays are thus recorded during SAR acquisition, according to the air column thickness (which is correlated with the topography) crossed by the radio wave. Hanssen (2001) even shows that the related interferometric phase errors can reach more than 35 mm for 2 points 2500 m vertically apart.

The general trend, related to the orbital errors and the tropospheric delay, is hence estimated by fitting a quadratic polynomial function on mean LOS velocities according to azimuths and elevations and is then removed (performed in a *MATLAB™* environment). Nevertheless, it did not improve our ability to detected large slope instabilities along the N7 corridor between Potrerillos and Uspallata, also as many points were masked out before this correction to unwrap the interferograms. More complex corrections included within the whole SBAS processing chain are indeed required and are currently under development (Lauknes 2011).

Moreover, a higher resolution DEM (other than the 30 m ASTER one that has too much artefact on those elevated areas) and some ground control points with 3D displacement time series would have been also necessary to better estimate these topography-related delays and to ensure reliable reference point locations. Completed with additional Envisat data, especially for 2007 and 2008, it would considerably improve the SBAS processing by reducing the temporal and normal baselines, as well as fringe unwrapping ambiguity issues. Unfortunately
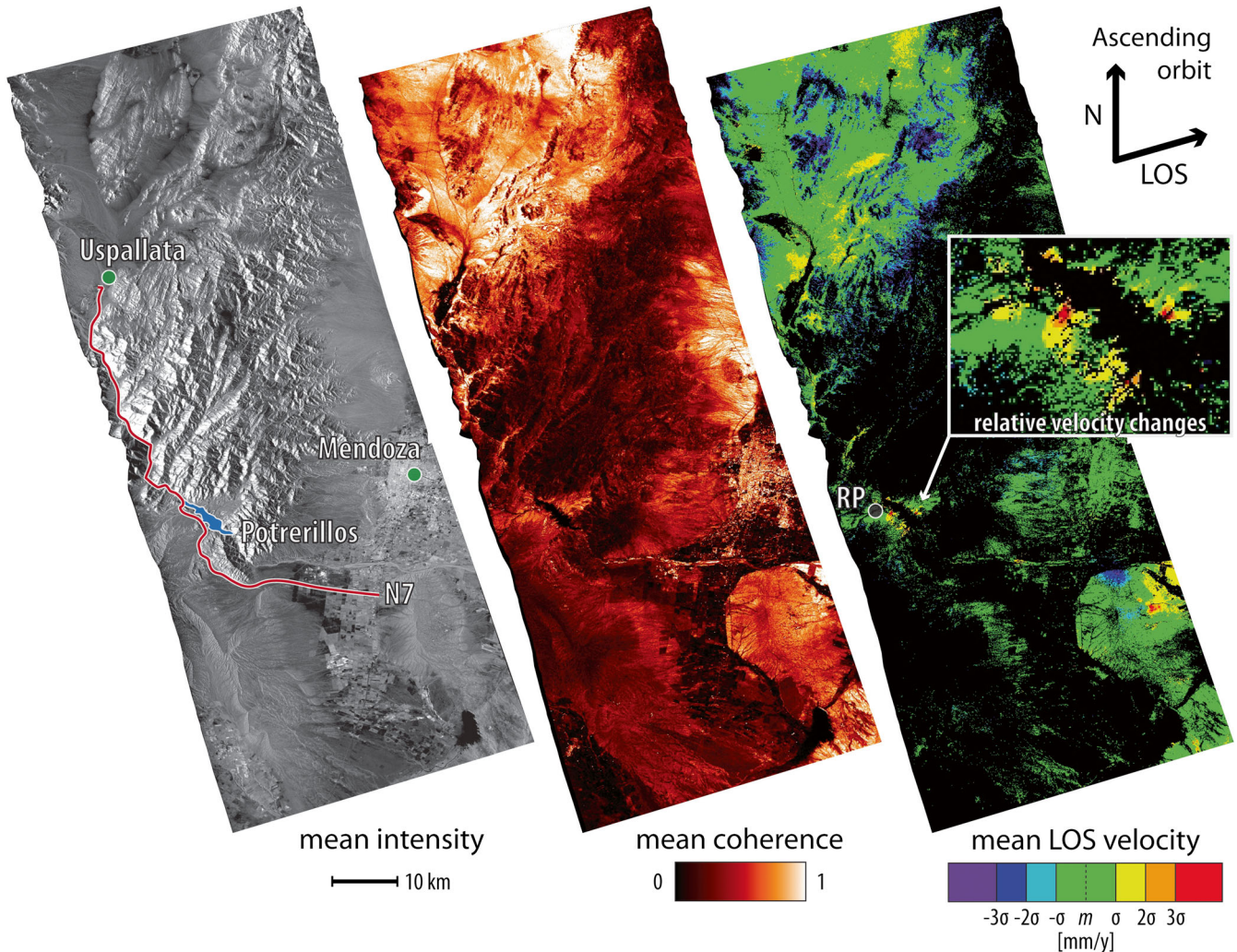
Fig. 5 *Left* Mean intensity of the 27 ascending scenes, *middle* mean coherences and *right* mean LOS velocities extracted from the SBAS processing of the 57 selected interferograms, with a median (*m*) of −1.4 mm/year and a standard deviation (*σ*) of 2 mm/year. Several downward mass movements along shore of the Potrerillos dam reservoir are noticed. In addition, other ground deformations are detected south of Mendoza close to oil extraction facilities. (*Positive values* downward displacements, away from the sensor; *negative values* upward displacements, toward the sensor. Raw Envisat data: ©*ESA 2010*)

these data, as well as ERS and ALOS ones, are not available for the study area.

SBAS-derived geometry

According to the Cruden and Varnes classification of landslides types (Cruden and Varnes 1996), both deformations can be identified as deep extremely slow soft rock slides. Both deformations indeed .involve weak sandstones and plastic clays of hundreds of metres deep (Folguera et al. 2003); they are moreover both extended over large areas, which let us assume that the main sliding surface is deep seated (Carter and Bentley 1985; Jaboyedoff and Derron 2015).

In addition, the geometry of the sliding surface can be derived from the SBAS results. Differences of displacement ranges of the eastern and western deformations observed on the ascending and descending processing can indeed be explained with simple geometrical considerations. A same true displacement vector indeed produces two distinct responses once projected on the two different ascending and descending LOS vectors that have look azimuth-angle of 074°27′ and 286°30′, respectively, according to Envisat orbits.

Regarding the western deformation, assuming a north-eastward movement (i.e. 025°, toward the reservoir) as suggested by its displacement gradient, a plunge of 34° is necessary on its upper part to reproduce the two measured ascending and descending SBAS responses. Moreover, a plunge of 05° in its lower part of this instability would be orthogonal to the descending LOS, explaining why no displacements are here detected on descending interferograms. The variation of the azimuth plunge from 025°34′ in the upper part to 025°05′ to its toe seems to indicate a general rotation of the mass movement.

In the meantime, regarding the eastern deformation, a horizontal south-westwards displacement (i.e. 200°00′) would also be almost orthogonal to the descending LOS. The detection of this mass movement would here again be hampered in that geometry, explaining why the displacement is detected on the ascending results but not on the descending ones. A near horizontal
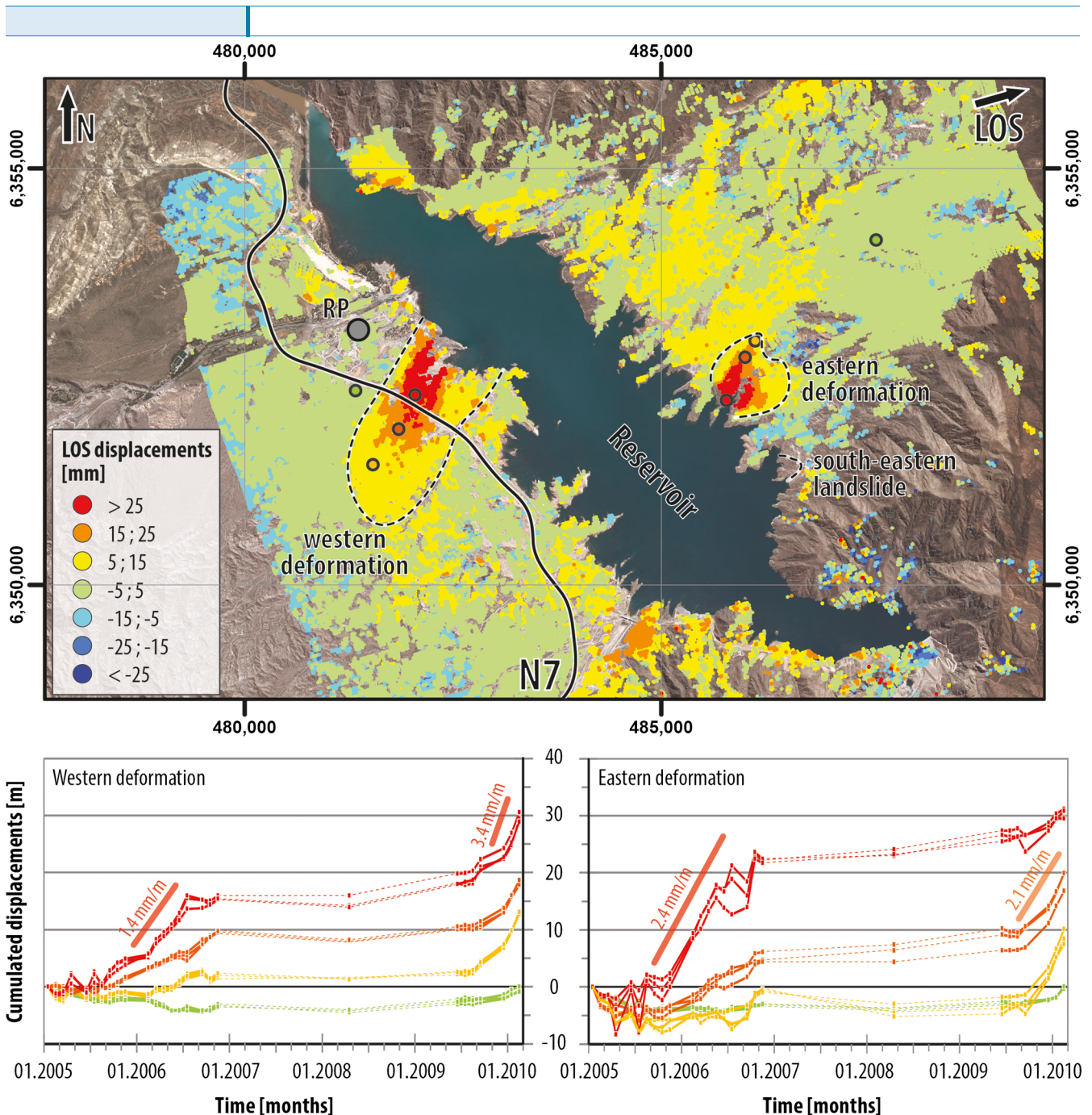
Fig. 6 *Up* LOS$_{ascending}$ cumulated displacements and location of the three major surface displacements detected along the Potrerillos reservoir shoreline. *Down* Displacement time series from January 2005 to February 2010 (LOS$_{ascending}$ projection) of several reflectors (*coloured dots on map*) within the western and eastern deformations and mean velocities. The *dot lines* underline potential fringe unwrapping ambiguity issues. The south-eastern landslide refers to the one described in the 'General setting' section of the supplementary material. (*Positive values* downward displacements, away from the sensor; *negative values*: upward displacements, toward the sensor. Satellite image from ©GoogleEarth)

translational displacement would in this case suggest a slope spread behaviour (Hungr et al. 2014), which might be controlled by plastic clay deposits noticed here (cf. 'Reservoir-slope deformation interactions'; Folguera et al. 2003).

Reservoir–slope deformation interactions

We now compare the Potrerillos water level variations with displacements patterns of both monitored mass movements

(Fig. 9). In 2007 and 2008, no correlations between displacement rates and the reservoir level can be observed, due to severe fringe unwrapping ambiguity issues that misrepresent SBAS measurements. However, we can nevertheless notice two periods of high displacement rates from February 2005 to July 2006 and September 2009 to February 2010, which actually correspond to reservoir drawdown and filling periods.
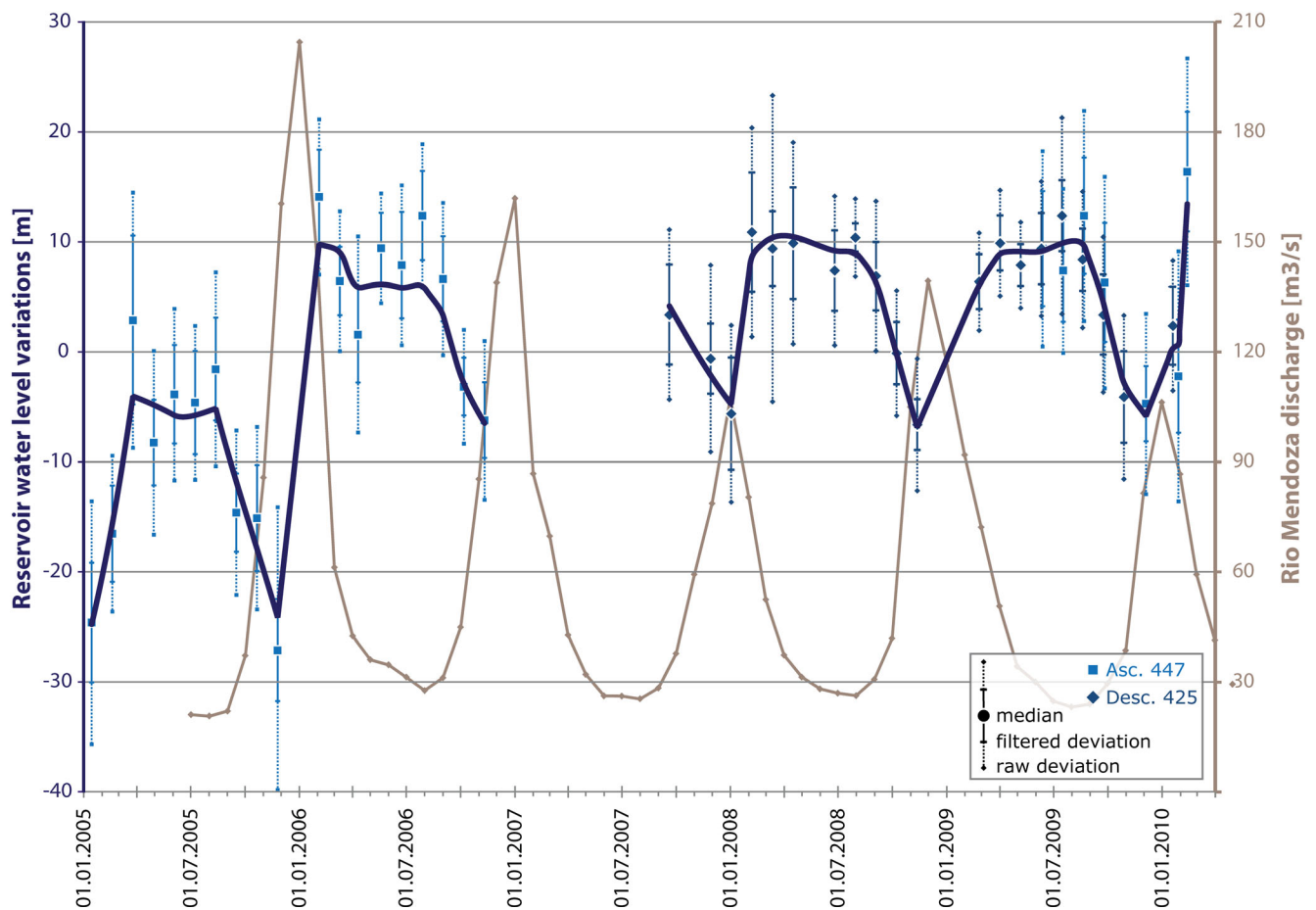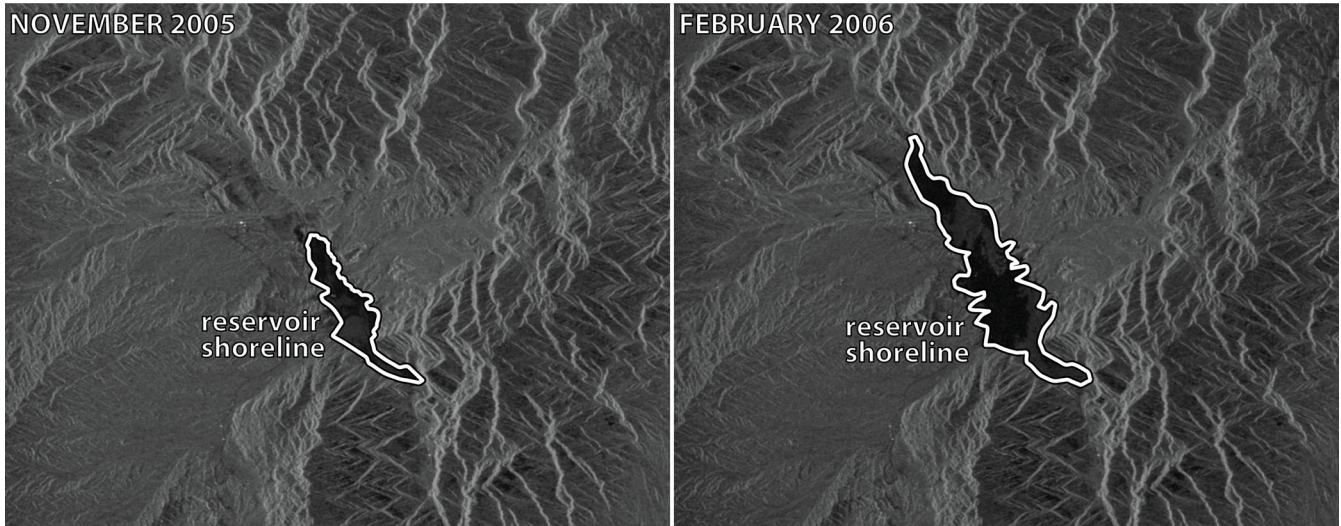
Fig. 7 *Up* Delimitations on SAR return amplitudes images of the Potrerillos reservoir shorelines during low and high water level periods (November 2005 and February 2006 respectively). *Down* Potrerillos reservoir level fluctuations extracted from SAR return amplitude images compared to Río Mendoza discharge. (Raw Envisat data: ©ESA 2010; Río Mendoza discharge data at the Guido station: ©*Subsecretaría de Recursos Hídricos*)

It therefore seems that deformation behaviours are actually modified in case of drawdown or filling.

In comparison to the relatively stable periods from June to August 2009, velocities indeed increase till about 0.8 mm/month during the reservoir drawdown from October to December; later, from end of August to beginning of October and from December to February 2010, during filling periods, velocities increase up to about 2.7 mm/month. The same pattern can also be noticed
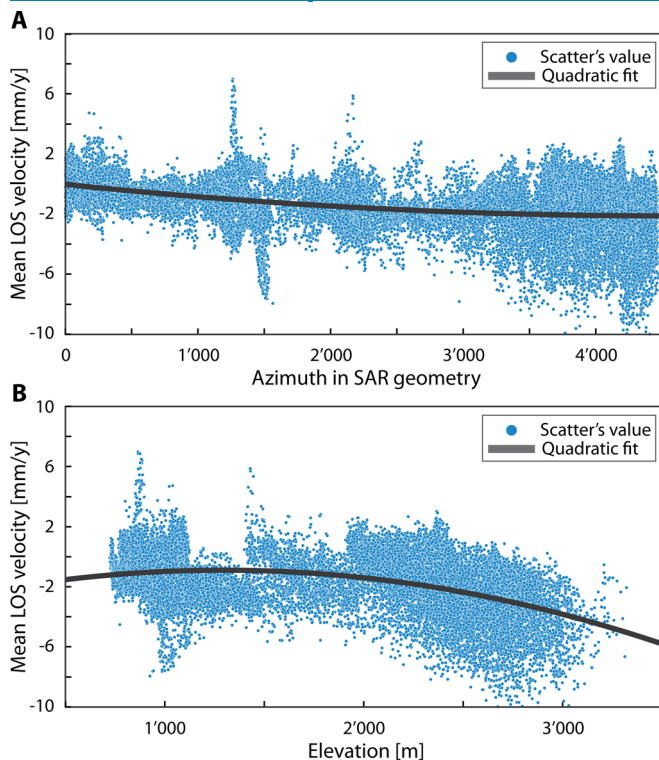
Fig. 8 a Mean LOS velocities vs. azimuth plot, as well as **b** mean LOS velocities vs. elevation plot, and their quadratic trends. Data are extracted from the ascending SBAS processing, displaying 1/75 of points

between August 2005 and July 2006. Moreover, we observe that high displacement rates continue from mid-April to July 2006, i.e. during 2.5 months after the stabilisation of the water level to its highest level reached for the first time. In addition, all displacements are measured downwards, and no up and down fluctuations due soil swelling and drying associated to cyclic water level variations are observed.

According to the geological local map (Folguera et al. 2003), the western and eastern slope deformations are both developed on tertiary rocks, i.e. hundreds metres thick fine sandstones layers regularly interlayered with thin clay deposits and coarse conglomerates, and are locally covered by superficial Quaternary sedimentary breccia deposits. Destabilising effects of reservoir drawdown have been reported in such lithologies, e.g. by Terzaghi (1950) or in Canelles (Pinyol et al. 2012) where the drawdown-induced landslide is mainly controlled by the low permeability and high plasticity of interlayered clay deposits. In addition, as reported in Riemer (1995) and Bell (2007) in such lithological contexts, sliding surfaces are frequently activated since water tables that significantly rise with reservoir filling may saturate bank materials, reducing the residual strength of shale surfaces and developing severe hydrostatic uplift pressure at the shale-sandstone contacts. Moreover, some delay between filling and displacements might also be observed and explained by usual low permeability and high capillarity of the fine sandstones (Bell 2007) that slow down the water table rising in these unsaturated materials.

In the meantime, the semi-arid conditions at Potrerillos are characterised by low annual cumulated rainfalls of about 200 mm/ year between 2004 and 2012 (Subsecretaría de Recursos Hídricos 2013). Summer periods, when most of the rain is recorded (Fig. 9), correlate with reservoir filling periods due to the Río Mendoza high discharge from snow melting in the high river watershed (cf. 'Water level fluctuations of the reservoir'); no conclusions on rainfall–landslide interactions can then be extracted from displacements time series. Moreover, there is no pre-dam construction reliable SAR data (cf. 'Limitations to large landslides detection' to really investigate rainfall effects on both landslides excluding the reservoir fluctuation level one. It nevertheless seems that rainfalls are not noticeably destabilising these soft rocks, since the semi-arid conditions could not saturate deep and large landslide masses and above all since no other landslides are detected in the same geological formation outside the reservoir shores.

The stability of the tertiary deposits seems to be therefore very sensitive to significant reservoir level variations, and detailed geotechnical investigations on the field are at this point mandatory to validate this statement.

Conclusions

The present study aimed to detect large slope deformations using a small baseline InSAR approach (Berardino et al. 2002; Lauknes et al. 2010) along the N7 between Potrerillos and Uspallata since the road is exposed to many natural hazards (Baumann et al. 2005). The Norut GSAR software (Larsen et al. 2005) has been used to process the 27 ascending and the 20 descending SAR scenes acquired by the Envisat satellite (Fig. 3).

As a result, the regional landslide detection processing did not highlight any large instability along steep elevated slopes of the N7 corridor (Fig. 5); this outcome does not mean that there is no landslide in this area, but if it does, they are not detected with our input dataset. The major part of pixels within the corridor were indeed (a) invisible from current LOS due to the steep geometry creating shadow radiometric distortion and (b) were also masked out because of very low coherences created by strong tropospheric delays and long snow cover periods on elevated areas. Both additional 2007–2008 SAR data to reduce temporal baselines as well as unwrapping ambiguities and DEM with higher resolutions to enhance topography-related correction would thus be necessary to improve the landslide detection capability.

Nevertheless, two unsuspected deep extremely slow soft rock slides were detected on gentle shores of the Potrerillos dam reservoir; both have main displacement directions toward the reservoir, with mean velocities up to 8 mm/year during the 2005–2006 period and up to 20 mm/year in 2009 (Fig. 6). After having extracted real displacements vectors from ascending and descending LOS results, a translational sliding surface is assumed for the eastern deformation, while a rotational component is suspected for the western deformation. In addition, a third active landslide not detected by InSAR (but described in 'General setting' of the supplementary material and recently presented by Sales et al. 2014) was identified on
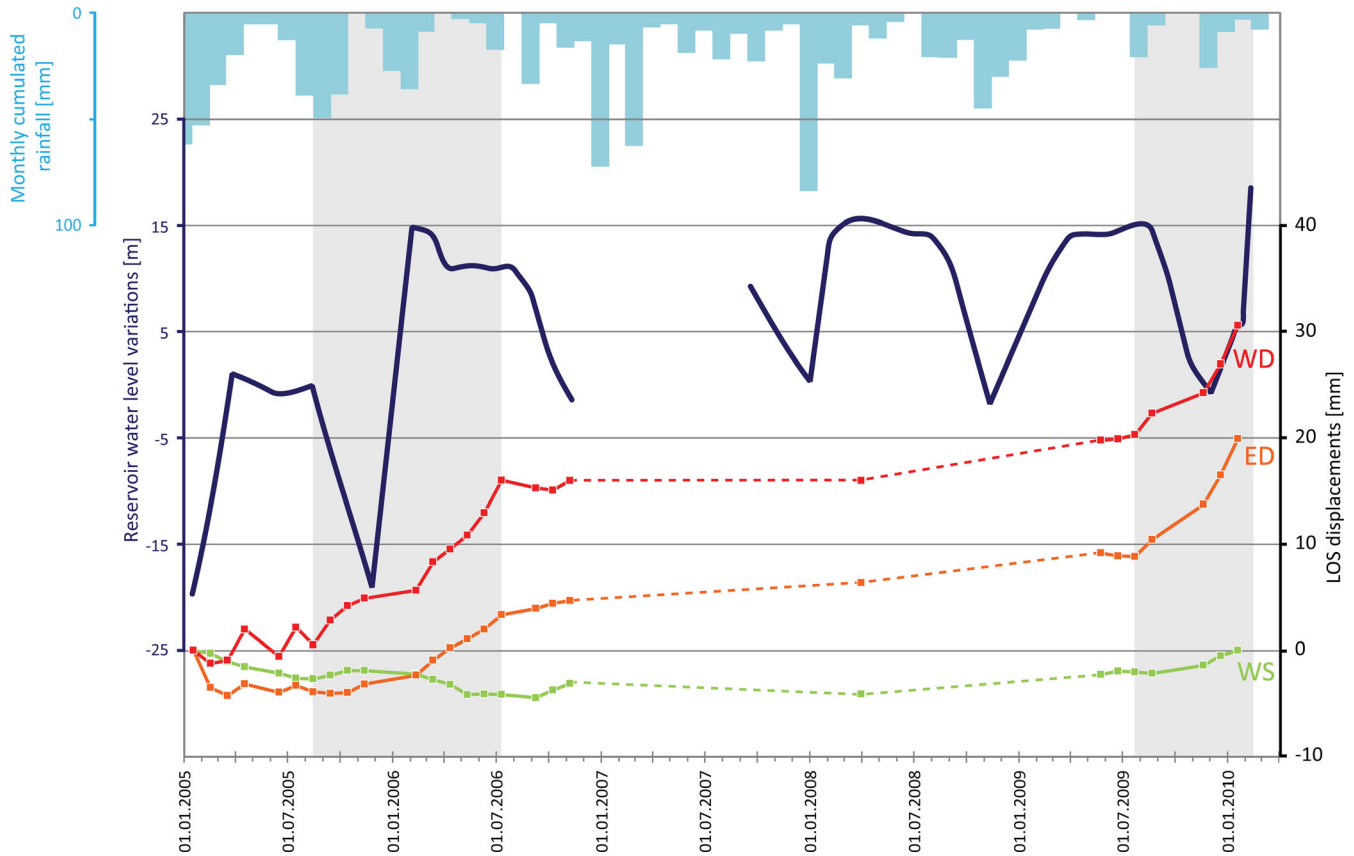
Fig. 9 Potrerillos reservoir water level variations and monthly cumulated rainfalls compared to cumulated displacements of scatters from the western (WD) and eastern (ED) deformations as well as from a stable part close to the western landslide (WS). The dot lines underline potential fringe unwrapping ambiguity issues. The 2 grey columns are overlapped with displacement acceleration periods. (Potrerillos rainfall data: ©*Subsecretaría de Recursos Hídricos*)

successive satellite imaging available on *Google™ Earth* showing retrogression of backscarps up to 20 m in 10 years and a general flow of the lower land part of 13 m in 2 years toward the lake.

In order to consider potential reservoir–landslide interactions, the water level variation of the Potrerillos dam reservoir was later assessed, after having extracted from the SRTM DEM the elevation of shoreline pixels isolated on the return amplitude signal of all SAR images (Fig. 7). Although no formal statement can be got from this study, there is however a body of evidences that the three large slope deformations (mainly composed of sandstones and clays) are actually influenced by the Potrerillos reservoir level variations.

To sum up, we show that very precise information on ground surface displacements above all coupled with an original reservoir water level variation survey can be extracted from spaceborne InSAR techniques (Fig. 9). In addition, detailed geological and rheological investigations, with also displacement and water table monitoring, can thus be planned from this study to (a) investigate in detail landslide destabilising factors and triggering mechanisms

and (b) forecast if necessary direct consequences of deformations and indirect ones of potential landslide impulse waves on infrastructures and populations.

References

Agliardi F, Crosta GB, Zanchi A (2001) Structural constraints on deep-seated slope deformation kinematics. Eng Geol 59:83–102

Ardizzone F, Cardinali M, Galli F, Guzzetti F, Reichenbach P (2007) Identification and mapping of recent rainfall-induced landslides using elevation data collected by airborne Lidar. Nat Hazards Earth Syst Sci 7:637–650

Bamler R, Hart P (1998) Synthetic aperture radar interferometry. Inverse Problems 14:R1–R54

Bardi B, Frodella W, Ciampalini A, Bianchini S, Del Ventisette C, Gigli G, Fanti R, Moretti S, Basile G, Casagli N (2014) Integration between ground based and satellite SAR data in landslide mapping: the San Fratello case study. Geomorphology 223:45–60

Baumann V, Coppolecchia M, González MA, Fauqué LE, Rosas M, Altobelli S, Wilson C, Hermanns RL (2005) Landslide processes in the Puente del Inca region, Mendoza, Argentina. In: Hungr O, Fell R, Couture R, Eberhardt E (eds) Proceedings of the International Conference on Landslide Risk Management, Vancouver, Canada. A.A. Balkema Publishers, London, Supplementary Volume (CD), pp 61–62

Baumann V, Wick E, Horton P, Jaboyedoff M (2011) Debris flow susceptibility mapping at a regional scale along the National Road N7, Argentina. In: Proceedings of the 2011 Pan-Am CGS Geotechnical Conference, Toronto, Canada, 7 p

Bell FG (2007) Engineering geology, 2nd edn. Butterworth-Heinemann, Oxford, UK

Berardino P, Fornaro G, Lanari R, Sansosti E (2002) A new algorithm for surface deformation monitoring based on small baseline differential SAR interferograms. IEEE Trans Geosci Remote Sens 40(11):2375–2383

Berardino P, Costantini M, Franceschetti G, Iodice A, Pietranera L, Rizzo V (2003) Use of differential SAR interferometry in monitoring and modelling large slope instability at Maratea (Basilicata, Italy). Eng Geol 68:31–51

Bianchini S, Cigna F, Righini G, Proietti C, Casagli N (2012) Landslide hotspot mapping by means of persistent scatterer interferometry. Environ Earth Sci 67:1155–1172

Braathen A, Blikra LH, Berg SS, Karlsen F (2004) Rock-slope failures in Norway; type, geometry, deformation mechanisms and stability. Nor J Geol 84:67–88

Carnec C, Massonnet D, King C (1996) Two example of the use of SAR interferometry on displacement fields of small spatial extent. Geophys Res Lett 23(24):3579–3582

Carter M, Bentley SP (1985) A procedure to locate slip surface beneath active landslides using surface monitoring data. Comput Geotech 1:139–153

Cascini L, Fornaro G, Peduto D (2009) Analysis at medium scale of low-resolution DInSAR data in slow-moving landslide-affected areas. ISPRS J Photogramm Remote Sens 64:598–611

Chen CW, Zebker HA (2001) Two-dimensional phase unwrapping with use of statistical models for cost functions in nonlinear optimization. J Opt Soc Am 18(2):338–351

Chigira M (1992) Long-term gravitational deformation of rocks by mass rock creep. Eng Geol 32:157–184

Chigira M, Duan F, Yagi H, Furuya T (2004) Using an airborne laser scanner for the identification of shallow landslides and susceptibility assessment in an area of ignimbrite overlain by permeable pyroclastics. Landslides 1:203–209

Cigna F, Bianchini S, Casagli N (2013) How to assess landslide activity and intensity with persistent scatterer interferometry (PSI): the PSI-based matrix approach. Landslides 10:267–283

Colesanti C, Wasowski J (2006) Investigating landslides with space-borne synthetic aperture radar (SAR) interferometry. Eng Geol 88:173–199

Cortés JM, Casa A, Pasini M, Yamín M, Terrizzano C (2006) Fajas oblicuas de deformación neotectónica en Precordillera y Cordillera Frontal (31°30′–33°30′): Controles paleotectónicos. Rev Asoc Geol Argent 61:639–646

Crosta GB, Frattini P, Agliardi F (2013) Deep seated gravitational slope deformations in the European Alps. Tectonophysics 605:13–33

Cruden D, Varnes D (1996) Landslides types and processes. In: Turner A, Schuster R (eds). Landslides, investigations and mitigations, transportation research board, special report 247, Washington, DC, pp 36–75

Dirección Nacional de Vialidad (2013) Road traffic statistics. http://transito.vialidad.gov.ar:8080/SelCE_WEB/intro.html2013. Accessed 6 Nov 2013

Doin MP, Lasserre C, Peltzer G, Cavalié O, Doubre C (2009) Corrections of stratified tropospheric delays in SAR interferometry: validation with global atmospheric models. J Appl Geophys 69:35–50

Fauqué L, Cortés JM, Folguera A, Etcheverría M (2000) Avalanchas de roca asociadas a neotectónica en el valle del río Mendoza, al sur de Uspallata. Rev Asoc Geol Argent 55:419–423

Fauqué L, Baumann V, Rosas M, González MA, Coppolecchia M, Di Tommaso I, Wilson CGJ (2005) Natural dams in the Mendoza River Basin, Mendoza Province, Argentina. Argentina. In: Hungr O, Fell R, Couture R, Eberhardt E (eds) Proceedings of the International Conference on Landslide Risk Management, Vancouver, Canada. A.A. Balkema Publishers, London, CD

Fell R, Corominas J, Bonnard C, Cascini L, Leroi E, Savage WZ, on behalf of the JTC-1 Joint Technical Committee on Landslides and Engineered Slopes (2008) Guidelines for landslide susceptibility, hazard and risk zoning for land use planning. Eng Geol 102:85–98

Fernández García F, Polimeni M (2003) Características Climáticas de los valles del Río Aconcagua (Chile) y del Río Mendoza (Argentina). In: Fernández García F, Mikkan R (eds) Evaluación Global del Medio Geográfico como base de un ordenamiento racional en el principal corredor Bioceánico del Plan Mercosur: Valles del Río Mendoza (Argentina) y Aconcagua (Chile). Universidad Nacional de Cuyo-Universidad Autónoma de Madrid, Mendoza, pp 88–92

Ferretti A, Prati C, Rocca F (2001) Permanent scatterers in SAR interferometry. IEEE Trans Geosci Remote Sens 39(1):8–20

Ferretti A, Fumagalli A, Novali F, Prati C, Rocca F, Rucci A (2011) A new algorithm for processing interferometric data-stacks: SqueeSAR. IEEE Trans Geosci Remote Sens 49(9):3460–3470

Folguera A, Etcheverría M, Pazos PJ, Giambiagi L, Fauqué L, Cortés JM, Rodríguez MF, Irigoyen MV, Fusari C (2003) Hoja Geológica 3369–15, Potrerillos, Provincia de Mendoza, 1:100 000. Instituto de Geología y Recursos Minerales, Servicio Geológico Minero Argentino, Buenos Aires

Fornaro G, Pauciullo A, Serafino F (2009) Deformation monitoring over large areas with multipass differential SAR interferometry: a new approach based on the use of spatial differences. Int J Remote Sens 30(6):1455–1478

Fruneau B, Apache J (1996) Observation and modelling of the Saint-Etienne-de-Tinée landslide using SAR interferometry. Tectonophysics 265:181–190

Fu W, Guo H, Tian Q, Guo X (2010) Landslide monitoring by corner reflectors differential interferometry SAR. Int J Remote Sens 31(24):6387–6400

Gabriel AK, Goldstein RM, Zebker HA (1989) Mapping small elevation changes over large areas: differential radar interferometry. J Geophys Res 94:9183–9191

Gansser A (1973) Facts and theories on the Andes. J Geol Soc 129:93–131

García-Davalillo J, Herrera G, Notti D, Strozzi T, Álvarez-Fernández I (2014) DInSAR analysis of ALOS PALSAR images for the assessment of very slow landslides: the Tena Valley case study. Landslides 11:225–246

Giambiagi L, Martinez AN (2008) Permo-Triassic oblique extension in the Potrerillos-Uspallata area, western Argentina. J S Am Earth Sci 26:252–260

Giambiagi L, Mescua J, Bechis F, Martinez A, Folguera A (2011) Pre-Andean deformation of the Precordillera southern sector, southern Central. Geosphere 7:219–239

Guzzetti F, Mondini AC, Cardinali M, Fiorucci F, Santangelo M, Chang KT (2012) Landslide inventory maps: new tools for an old problem. Earth Sci Rev 112:42–66

Hanssen RF (2001) Radar Interferometry: data interpretation and error analysis. Kluwer Academic Publishers, Dordrecht

Henderson IHC, Lauknes TR, Osmundsen PT, Dehls J, Larsen Y, Redfield TF (2011) A structural, geomorphological and InSAR study of an active rock slope failure development. In: Jaboyedoff (ed) Slope tectonics, vol 351. Geological Society, London, pp 185–189

Hermanns RL, Fauqué L, Wilson CGL (2014) 36Cl terrestrial cosmogenic nuclide dating suggests Late Pleistocene to Early Holocene mass movements on the south face of Aconcagua mountain and in the Las Cuevas–Horcones valleys, Central Andes, Argentina. In: Sepúlveda, Giambiagi, Moreiras, Pinto, Tunik, Hoke, Farías (eds) Geodynamic processes in the Andes of Central Chile and Argentina, Geological Society, London, 24 p

Herrera G, Notti D, García-Davalillo JC, Mora O, Cooksley G, Sánchez M, Arnaud A, Crosetto M (2011) Analysis with C- and X-band satellite SAR data of the Portalet landslide area. Landslides 8:195–206

Herrera G, Gutiérrez F, García-Davalillo JC, Guerrero J, Notti D, Galve JP, Fernández-Merodo JA, Cooksley G (2013) Multi-sensor advanced DInSAR monitoring of very slow

landslides: the Tena Valley case study (Central Spanish Pyrenees). Remote Sens Environ 128:31–43

Höhle J, Höhle M (2009) Accuracy assessment of digital elevation models by means of robust statistical methods. ISPRS J Photogramm Remote Sens 64:398–406

Hungr O, Leroueil S, Picarelli L (2014) The Varnes classification of landslide types, an update. Landslides 11:167–194

Jaboyedoff M, Derron MH (2015) Methods to estimate the surfaces geometry and uncertainty of landslide failure surface. In: Lollino G et al. (Eds.) Engineering geology for society and territory. Proceedings of the IAEG XII Congress, Torino, Italy, 15–19 September 2014, 2:339–343

Jaboyedoff M, Choffet M, Derron MH, Horton P, Loye A, Longchamp C, Mazotti B, Michoud C, Pedrazzini A (2012) Preliminary slope mass movements susceptibility mapping using DEM and LiDAR DEM. In: Pradhan B (ed) Terrigenous mass mouvements. Springer, Berlin Heidelberg, pp 109–169

Jarvis A, Reuter HI, Nelson A, Guevara E (2008) Hole-filled seamless SRTM data V4. International Centre for Tropical Agriculture. http://srtm.csi.cgiar.org. Accessed 31 Mar 2014

Kendrick EC, Bevis M, Smalley RF Jr, Cifuentes O, Galban F (1999) Current rates of convergence across the Central Andes: estimates from continuous GPS observations. Geophys Res Lett 26(5):541–544

Kimura H, Yamaguchi Y (2000) Detection of landslide areas using satellite radar interferometry. Photogramm Eng Remote Sens 66(3):337–344

Kozlowski EE, Mancedo R, Ramos VA (1993) Geología y Recursos Naturales de Mendoza. In: Proceedings of the 12th Servicio Geológico Argentino Conference and 2nd Congreso de Exploración de Hidrocarburos, 1(18):235–256

Larsen Y, Eigen G, Lauknes TR, Malnes E, Høgda KA (2005) A generic differential interferometric SAR processing system, with applications to land subsidence and snowwater equivalent retrieval. In: Proceedings of the Fringe 2005 Workshop, Frascati, Italy, 28 November – 2 December 2005, 6 p

Lauknes TR (2011) InSAR tropospheric stratification delays: correction using a small baseline approach. IEEE Geosci Remote Sens Lett 8(6):1070–1074

Lauknes TR, Piyush Shanker A, Dehls JF, Zebker HA, Henderson IHC, Yarsen Y (2010) Detailed rockslide mapping in northern Norway with small baseline and persistent scatterer interferometric SAR time series methods. Remote Sens Environ 114:2097–2109

López F, Rodríguez A, Dölling OR (2011) Inventario de Presas y Centrales Hdroeléctricas de la República Argentina. Ministerio de la Planificación Federal. Inversión pública y Servicios, Buenos Aires, 224 p

Massonnet D (1985) Etude de Principe d'une Détection de Mouvements Tectoniques par Radar. Internal memo No. 326, Centre National d'Etude Spatial (CNES), Toulouse, France

Massonnet D, Feigl KL (1998) Radar interferometry and its applications to changes in the Earth's surface. Rev Geophys 36:441–500

Massonnet D, Rossi M, Carmona C, Adragna F, Peltzer G, Feigl K, Rabaute T (1993) The displacement field of the Landers earthquake mapped by radar interferometry. Nature 364:138–142

Massonnet D, Briole P, Arnaud A (1995) Deflation of Mount Etna monitored by spaceborne radar interferometry. Nature 375:567–570

McKean J, Roering J (2004) Objective landslide detection and surface morphology mapping using high-resolution airborne laser altimetry. Geomorphology 57:331–351

Moreiras SM (2005) Landslide susceptibility zonation in the Rio Mendoza Valley, Argentina. Geomorphology 66:345–357

Moreiras SM (2006) Frequency of debris flows and rockfall along the Mendoza river valley (Central Andes), Argentina: associated risk and future scenario. Quat Int 118:110–121

Müller L (1964) The rock slide in the Vaiont Valley. Rock Mech Eng Geol 2:148–212

Pedrazzini A (2012) Characterization of gravitational rock slope deformations at different spatial scales based on field, remote sensing and numerical approaches, PhD thesis of the University of Lausanne

Pinyol NM, Alonso EE, Corominas J, Moya J (2012) Canelles landslide: modelling rapid drawdown and fast potential sliding. Landslides 9:33–51

Polansky J (1963) Estratigrafía, neotectónica y geomorfología del Pleistoceno pedemontano entre los ríos Diamante y Mendoza. Asociación Geológica Argentina Revista 17:127–349

Ramos V (1997) El Segmento de Subducción Subhorizontal de los Andes Centrales Argentino-Chilenos. Acta Geol Hisp 32:5–16

Ramos VA (1999) Plate tectonic setting of the Andean Cordillera. Episodes 22(3):183–190

Rib HT, Liang T (1978) Recognition and identification. In: Schuster R and Krizek RJ (eds) Landslides, analysis and control. Transportation Research Board, Special Report 176, Washington DC, pp 34–80

Riemer W (1995) Keynote paper: landslides and reservoirs. In: Bell FG (ed) Landslides. Balkema, Rotterdam, pp 1973–2004

Sales DA, Moreiras SM, Gardini CE (2014) Análisis de estabilidad del deslizamiento rotacional en el cerro Los Baños, Potrerillos, Provincia de Mendoza, Argentina. XIX Congreso Geológico Argentino, Jujuy, Abstracts

Saroli M, Stramondo S, Moro M, Doumaz F (2005) Movements detection of deep seated gravitational slope deformations by means of InSAR data and photogeological interpretation: northern Sicily case study. Terra Nov. 17:35–43

Schuster RL (2006) Interaction of dams and landslides—case studies and mitigation. Professional Paper 1723, US Geological Survey

Shapiro II, Zisk SH, Rogers AEE, Slade MA, Thompson TW (1972) Lunar topography: global determination by radar. Delay-doppler stereoscopy and radar interferometry yield high-resolution three-dimensional views of the moon. Science 178(4064):939–948

Sigmundsson F, Vadon H, Massonnet D (1997) Readjustment of the Krafla spreading segment to crustal rifting measured by satellite radar interferometry. Geophys Res Lett 24(15):1843–1846

Singleton A, Li Z, Hoey T, Muller JP (2014) Evaluating sub-pixel offset techniques as an alternative to D-InSAR for monitoring episodic landslide movements in vegetated terrain. Remote Sens Environ 147:133–144

Squarzoni C, Delacourt C, Allemand P (2003) Nine years of spatial and temporal evolution of the La Valette landslide observed by SAR interferometry. Eng Geol 68:53–66

Stipanicic PN (1979) El Triásico del valle del Río de los Platos (Provincia de San Juan). In: Turner JCM (ed) Segundio Simposio de Geología Regional Argentina: Córdoba, Academia Nacional de Ciencias 1:695:744

Subsecretaría de Recursos Hídricos (2013) Rio Mendoza discharge. http://www.hidricosargentina.gov.ar. Accessed 11 Oct 2013

Tarayre H, Massonnet D (1996) Atmospheric propagation heterogeneities revealed by ERS-1 interferometry. Geophys Res Lett 23(9):989–992

Terzaghi K (1950) Mechanism of landslides. The Geological Society of America, Engineering Geology (Berkley) Volume, 83–123

Tomás R, Li Z, Liu P, Singleton A, Hoey T, Cheng X (2014) Spatiotemporal characteristics of the Huangtupo landslide in the Three Gorges region (China) constrained by radar interferometry. Geophys J Int. doi:10.1093/gji/ggu017, 20 p

Trombotto D, Borzotta E (2009) Indicators of present global warming through changes in active layer-thickness, estimation of thermal diffusivity and geomorphological observations in the Morenas Coloradas rockglacier, Central Andes of Mendoza, Argentina. Cold Reg Sci Technol 55:321–330

Wang F, Zhang Y, Huo Z, Peng X, Araiba K, Wang G (2008) Movement of the Shuping landslide in the first four years after the initial impoundment of the Three Gorges Dam Reservoir, China. Landslides 5:321–329

Wick E, Baumann V, Jaboyedoff M (2010a) Brief communication: "Report on the impact of the 27 February 2010 earthquake (Chile, Mw 8.8) on rockfalls in the Las Cuevas valley, Argentina". Nat Hazards Earth Syst Sci 10:1989–1993

Wick E, Baumann V, Favre-Bulle G, Jaboyedoff M, Loye A, Marengo H, Rosas M (2010b) Flujos de detritos recientes en la cordillera frontal de Mendoza: Un ejemplo de riesgo natural en la ruta 7. Rev Asoc Geol Argent 66:460–465

Woodhouse IH (2006) Introduction to microwaves remote sensing. CRC Taylor & Francis, Boca Raton

Xia M, Ren GM, Ma XL (2013) Deformation and mechanism of landslide influenced by the effects of reservoir water and rainfall, Three Gorges, China. Nat Hazards 68:467–482

Yin Y, Zheng W, Liu Y, Zhang J, Li X (2010) Integration of GPS with InSAR to monitoring of the Jiaju landslide in Sichuan, China. Landslides 7:359–365

Záruba Q, Mencl V (1982) Landslides and their control: developments in geotechnical engineering 31. Academia Publishing House of the Czechoslovak Academy of Sciences, Prague

Zebker HA, Rosen PA, Hensley S (1997) Atmospheric effects in interferometry synthetic aperture radar surface deformation and topographic maps. J Geophys Res 102:7547–7563

C. Michoud (✉) · I. Penna · M.-H. Derron · M. Jaboyedoff
Institute of Earth Sciences,
University of Lausanne,
Géopolis, rue de la Mouline, 1015, Lausanne, Switzerland
e-mail: clement.michoud@terranum.ch

I. Penna
e-mail: ivanna.penna@unil.ch

M.-H. Derron
e-mail: marc-henri.derron@unil.ch

M. Jaboyedoff
e-mail: michel.jaboyedoff@unil.ch

C. Michoud
Terranum,
rue de l'industrie 35bis, Bussigny, Switzerland

V. Baumann
Geological Survey of Argentina,
Avda. General Paz 5445, B 1650-WAB, San Martín-Miguelete, Provincia de Buenos Aires, Argentina
e-mail: valerie.baumann@segemar.gov.ar

T. R. Lauknes
Norut,
P.O. Box 6434 Forskningsparken, 9294, Tromsø, Norway
e-mail: tom.rune.lauknes@norut.no